Customizing the Polarity of Single-Walled Carbon-Nanotube Field-Effect Transistors Using Solution-Based Additives

Salazar-Rios, Jorge Mario; Sengrian, Aprizal Akbar; Talsma, Wytse; Duim, Herman; Abdu-Aguye, Mustapha; Jung, Stefan; Froehlich, Nils; Allard, Sybille; Scherf, Ullrich; Loi, Maria Antonietta

Published in:
Advanced electronic materials

DOI:
10.1002/aelm.201900789

Publication date:
2020

ADVANCED ELECTRONIC MATERIALS
www.advelectronicmat.de

Customizing the Polarity of Single-Walled Carbon-Nanotube Field-Effect Transistors Using Solution-Based Additives

*Jorge Mario Salazar-Rios, Aprizal Akbar Sengrian, Wytse Talsma, Herman Duim, Mustapha Abdu-Aguye, Stefan Jung, Nils Fröhlich, Sybille Allard, Ullrich Scherf, and Maria Antonietta Loi**

Polarity control in semiconducting single-walled carbon-nanotube field-effect transistors (s-SWNT FETs) is important to promote their application in logic devices. The methods to turn the intrinsically ambipolar s-SWNT FETs into unipolar devices that have been proposed until now require extra fabrication steps that make preparation longer and more complex. It is demonstrated that by starting from a highly purified ink of semiconducting single-walled carbon nanotubes sorted by a conjugated polymer, and mixing them with additives, it is possible to achieve unipolar charge transport. The three additives used are benzyl viologen (BV), 4-(2,3-dihydro-1,3-dimethyl-1H-benzimidazol-2-yl)-*N*,*N*-dimethylbenzenamine (N-DMBI), which give rise to n-type field-effect transistors, and 2,3,5,6-tetrafluoro-7,7,8,8-tetracyanoquinodimethane (F_4-TCNQ) which gives rise to p-type transistors. BV and N-DMBI transform the s-SWNTs transistors from ambipolar with mobility of the order of 0.7 $cm^2 V^{-1} s^{-1}$ to n-type with mobility up to 5 $cm^2 V^{-1} s^{-1}$. F_4-TCNQ transform the ambipolar transistors in p-type with mobility up to 16 $cm^2 V^{-1} s^{-1}$.

1. Introduction

After their discovery in 1993, single-walled carbon nanotubes (SWNTs) have been extensively studied for their use in the fabrication of electronic devices. SWNTs are one of the most promising options to replace silicon as building blocks for transistor and complex logic circuits.[1]

Their outstanding charge transport,[2] high thermal stability, and robust mechanical properties raised many expectations about their applications in electronics. These expectations have stimulated a large number of investigations in the last two decades, where semiconducting SWNTs (s-SWNTs) are used as the active channel for field-effect transistors (FETs).[3–5]

However, when SWNTs are synthesized, the samples do not only contain semiconducting species (s-SWNTs) but include metallic ones as well.[6] The presence of metallic tubes is highly detrimental to the performance of FETs and has been limiting the application of SWNTs in electronics so far.[7,8]

An effective approach to removing such metallic species from SWNT samples is the polymer wrapping technique. In this technique, SWNTs are non-covalently functionalized by conjugated polymer chains in the presence of an organic solvent.[9] The interaction between the polymer chains and the walls of the s-SWNTs leads to the suspension of specific semiconducting species and allows in this way their selection.[10]

The inks composed of polymer sorted s-SWNT have been demonstrated to be of high quality and have allowed the fabrication of field-effect transistors of outstanding performances, namely, on/off ratio up to 10^8,[11] and mobilities above 30 $cm^2 V^{-1} s^{-1}$.[12,13] However, field-effect transistors using network s-SWNTs as active material generally display ambipolar behavior, weakening their utility for the fabrication of logic circuits.[14,15] Therefore, to be able to use SWNTs in inverters and other logic circuits, control over the FETs polarity needs to be achieved first.[16–25]

Several approaches have been demonstrated to provide control over the polarity of s-SWNTs FETs. These approaches involve the use of specific dielectric materials,[26] the introduction of a barrier for one of the carriers by choosing adequate source-drain metal contacts,[27] the use of new device architectures,[28] and the introduction of an extra doping layer deposited on top of the s-SWNT active channel.[18,29] All these approaches, unfortunately, require additional fabrication steps, making them in some respect inconvenient. Recently, we have demonstrated that by using conjugated polymers with different energy levels, it is possible to obtain field-effect transistors with an enhanced n- or p-type character.[11,30] However, these devices do not show perfect unipolar behavior. In contrast, the careful

Dr. J. M. Salazar-Rios,[+] A. A. Sengrian, W. Talsma, H. Duim, M. Abdu-Aguye, Prof. M. A. Loi
University of Groningen
Zernike Institute for Advanced Materials
Nijenborgh 4, 9747 AG Groningen, The Netherlands
E-mail: m.a.loi@rug.nl

Dr. S. Jung, Dr. N. Fröhlich, Dr. S. Allard, Prof. U. Scherf
Bergische Universität Wuppertal
Makromolekulare Chemie und Institut für Polymertechnologie
Gaußstraße 20, 42119 Wuppertal, Germany

The ORCID identification number(s) for the author(s) of this article can be found under https://doi.org/10.1002/aelm.201900789.

[+]Present address: Universidad de Manizales, Carrera 9a No 19-03, 170001 Manizales, Colombia

DOI: 10.1002/aelm.201900789

tuning of the number of SWNTs and the engineering of the device structure using P(VDF-TrFE-CFE) /PMMA as gate dielectric have led to the development of good p-type transistors, which have been used for the fabrication of hybrid inverters using PbS QDs as the n-type material. These inverters operate in the sub-1 V range (0.9 V) with gain up to 76 V per V, and display large maximum-equal-criteria noise margins of 80%.[31]

In this work, we present a strategy to control the polarity of carbon nanotube field-effect transistors, in a simple way, namely without increasing the number of fabrication steps. The strategy is to add an extra component directly to the purified s-SWNT ink, which is ready to be used for the fabrication of n- or p-type transistors.

To this purpose, we investigated s-SWNTs samples where benzyl viologen (BV), 4-(2,3-dihydro-1,3-dimethyl-1H-benzimidazol-2-yl)-*N*,*N*-dimethylbenzenamine (N-DMBI) and 2,3,5,6-tetrafluoro-7,7,8,8-tetracyanoquinodimethane (F_4-TCNQ) have been used as additives during the ink preparation procedure. BV and N-DMBI are found to induce electron dominated transport in the FETs while F_4-TCNQ is enhancing the hole transport with hole mobility reaching up to 16 $cm^2\ V^{-1}\ s^{-1}$. The mechanism of the variation of the device performance is investigated by comparing planar and staggered device structures. BV is found to influence the work function of the metal, while N-DMBI and F_4-TCNQ are found to dope the active layer. In particular, F_4-TCNQ doping of the s-SWNTs is mediated by the wrapping polymer.

2. Results and Discussion

HiPCO (high-pressure CO method) nanotubes and the conjugated polymer poly(3-dodecylthiophene-2,5-diyl) (P3DDT) are used to prepare the well-characterized HiPCO:P3DDT inks, which have a high dispersion yield and show high purity of semiconducting tubes.[32,33] The inks were prepared using the procedure described in Section 4 and reported earlier by Gomulya et al.[33] Additionally, the inks contain different chiralities, as evident from the absorption spectra. This is a further difficulty in finding dopants, as the variation of energy levels from tube-to-tube can change the doping efficiency. Therefore, our purpose is to demonstrate that also polychirality samples can be doped and used for low-cost electronics

The output characteristics of the FETs fabricated with the pristine inks in a coplanar transistor structure, composed by a SiO_2 layer acting as gate dielectric and Au as drain/source electrodes (**Figure 1**a), are reported in Figure 1b. Even though s-SWNTs are intrinsically ambipolar,[14,34] the P3DDT polymer acts as an electron acceptor[35] making the transport properties of the SWNT-polymer hybrids p-type dominated,[11] as is visible in the output curve reported in Figure 1b. Even though these transistors show p-type dominated transport with an average hole mobility of 2.4 $cm^2\ V^{-1}\ s^{-1}$, electron transport is still present with a mobility of 0.7 $cm^2\ V^{-1}\ s^{-1}$ (see Figure S1, Supporting Information, for the transfer characteristics).

At this point, it is important to mention, that while we have demonstrated earlier that by using n-type polymers it is possible to fabricate n-type dominated SWNT FETs, also in those

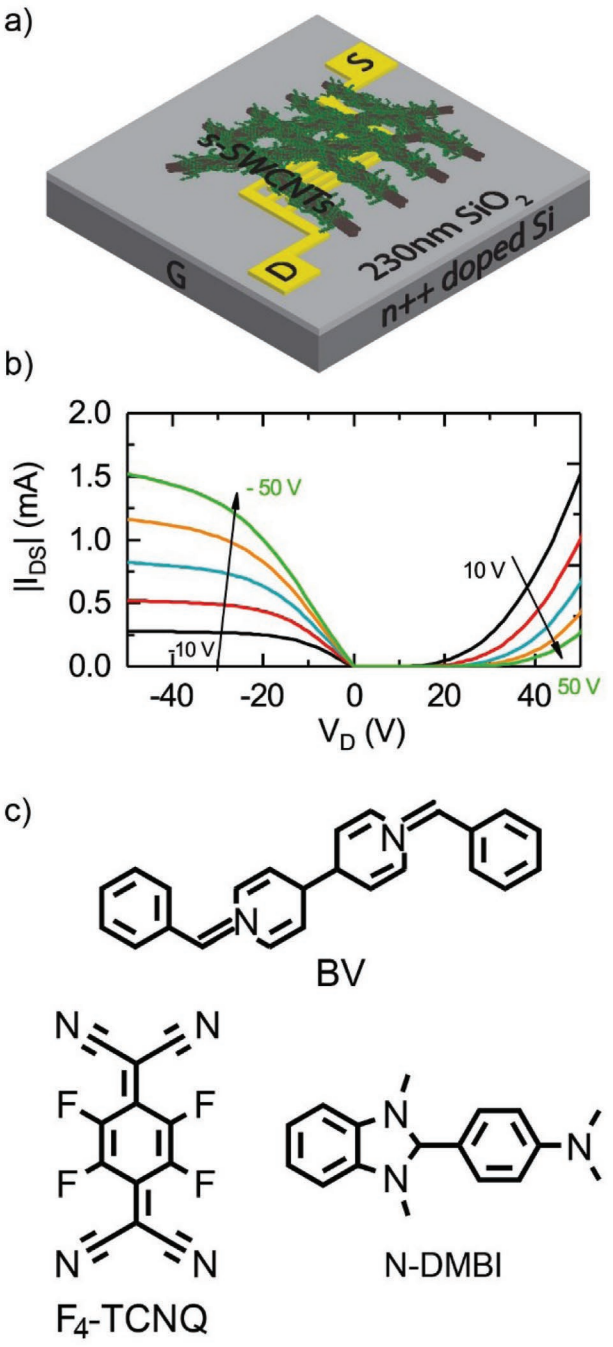

Figure 1. a) Coplanar (bottom gate, bottom contacts) FET structure. b) Output curve of the reference HiPCO:P3DDT FET showing p-type dominated transport. c) Chemical structure of BV, F_4-TCNQ, and N-DMBI.

samples the electrical characteristics still display ambipolar character.[30]

The fabrication of efficient complementary devices requires the availability of both p- and n-type field-effect transistors, with minimal contribution from the charge carriers of opposite sign in each of these devices. We therefore search for additives, with the aim to transform the ambipolar inks in n- and p-type ones. Two molecules that are known for improving the n-type transport, namely N-DMBI[18] and BV,[36] and a molecule that is

known for its p-type doping capacity F_4-TCNQ[37] were selected for this experiment. The chemical structures of the three molecules are depicted in Figure 1c.

N-DMBI and F_4-TCNQ were solubilized in o-xylene, while the neutral BV molecules were extracted using the method reported by Kim et al. and then solubilized in o-xylene.[36] Then the dopant solutions were mixed singularly with the HiPCO:P3DDT ink and treated as described in Section 4.

As we are adding organic molecules to our colloidally stable ink of s-SWNTs, the first step is to investigate the absorption spectra of the new solutions to be sure that the colloidal stability is not being affected. When the n-type additives, N-DMBI and BV are used, the absorption spectra of the SWNTs hybrid appear unaffected (Figure S2, Supporting Information). A totally different situation arises when F4-TCNQ is added to the HiPCO:P3DDT dispersion. **Figure 2**a shows the absorption spectra of solutions containing increasing concentrations of F_4-TCNQ. The sharp peaks presented by the reference sample in the near-infrared region correspond to the first excitonic absorption transition (S_{11}) of the different individualized s-SWNTs chiralities. When F_4-TCNQ is added, the spectra show a strong loss of the oscillator strength of the S_{11} transition for all chiralities. Moreover, large variations are also evident in the high-energy part of the spectra corresponding to the conjugated polymer absorption, which, in stark contrast to the SWNTs, gains in oscillator strength. It is interesting that in this spectral region the signature of the free polymer chains becomes evident upon the addition of F_4-TCNQ (vide infra).[33]

To further understand the nature of these variations in the absorption spectra, steady-state and time-resolved (TR) photoluminescence (PL) measurements of the HiPCO:P3DDT inks with and without 0.181 mM F_4-TCNQ were performed. The PL of the S_{11} s-SWNTs is completely quenched which indicates the opening of a very efficient non-radiative recombination channel when F_4-TCNQ is present. This might be related to the formation of trions.[38] However, F_4-TCNQ appears not only to interact with the carbon nanotubes but also to disrupt the wrapping of the polymer and to interact directly with the polymer chains. As mentioned above, larger absorption from P3DDT isolated chains upon addition of F_4-TCNQ is appearing. This indicates that the dopant is interfering with the interaction between the polymer and the single tubes.

The PL intensity of the P3DDT present in the nanotube ink is reduced substantially (Figure 2b), and its photoluminescence decay time from monoexponential becomes biexponential (Figure 2c). These results indicate that the interaction of F_4-TCNQ with the SWNTs is (partially) mediated by the polymer. However, only the study of the transport properties in field-effect transistors can clarify if the three selected molecules act as dopants for SWNTs and if, in the case of F_4-TCNQ, the polymer is really disconnected from the SWNT, with the consequent variation of their concentration in solution.

Figure 3a shows the output curves of two FETs, one prepared with the HiPCO:P3DDT ink mixed with 370 µM N-DMBI (top), and the other prepared with the HiPCO:P3DDT ink mixed with 15 µM BV (bottom). The output curves show that after adding N-DMBI and BV, the device polarity changed from p-type (Figure 1b) to n-type dominated for both devices.

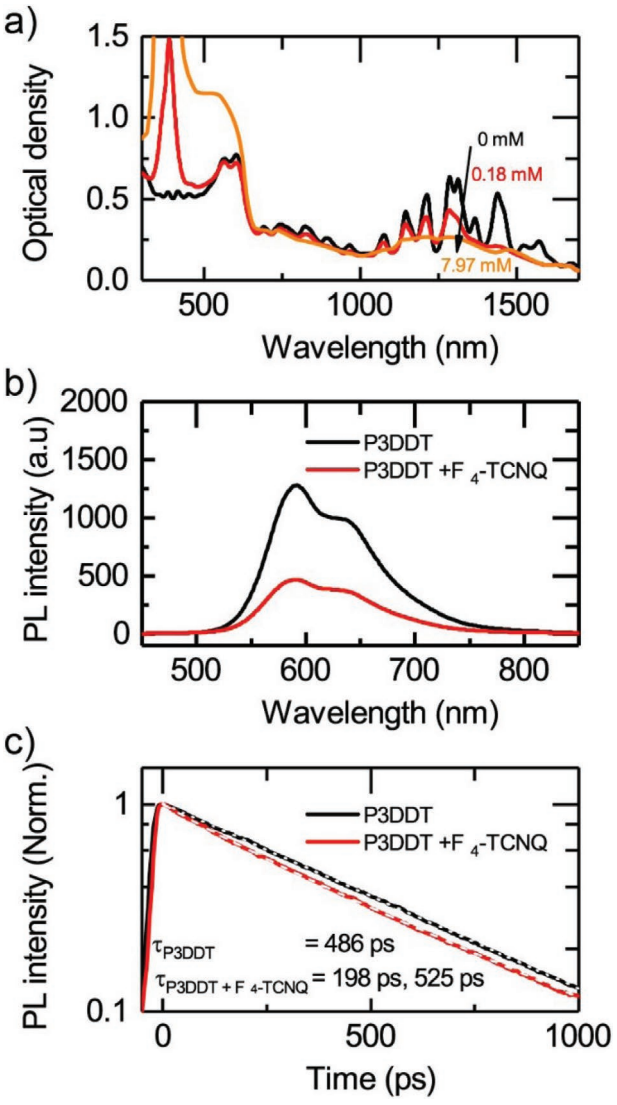

Figure 2. a) Absorption spectra of the reference ink HiPCO:P3DDT and the inks containing different concentrations of F_4-TCNQ. The absorption of pristine F_4-TCNQ is presented in Figure S3, Supporting Information; b) steady-state PL of the P3DDT present in the HiPCO:P3DDT ink with (red) and without (black) 0.18 mM F_4-TCNQ. c) Time-resolved PL of the P3DDT present in the HiPCO:P3DDT ink with (red) and without (black) the 0.18 mM F4-TCNQ. The dashed white lines are the exponential fits.

The electron mobility of the devices with N-DMBI and BV are 4.2 ± 0.7 cm^2 V^{-1} s^{-1} and 2.5 ± 0.4 cm^2 V^{-1} s^{-1}, respectively, which are respectively 6 and 4 times higher than the electron mobility of the reference device (0.7 ± 0.2 cm^2 V^{-1} s^{-1}). For devices with the maximum additive concentration, it is not possible to calculate the hole mobility. However, for devices with 1.5 µM BV and 37 µM N-DMBI, the hole mobility is as low as 10^{-4} cm^2 V^{-1} s^{-1}, which is five orders of magnitude lower than the hole mobility of the reference device (2.4 ± 0.4 cm^2 V^{-1} s^1).

Figure 3b shows the transfer curves of the transistors prepared with HiPCO:P3DDT ink mixed with different concentrations of either N-DMBI (top) or BV (bottom). At increasing concentrations of N-DMBI as well as of BV, the plots exhibit a large variation of the threshold voltage (V_{TH}).

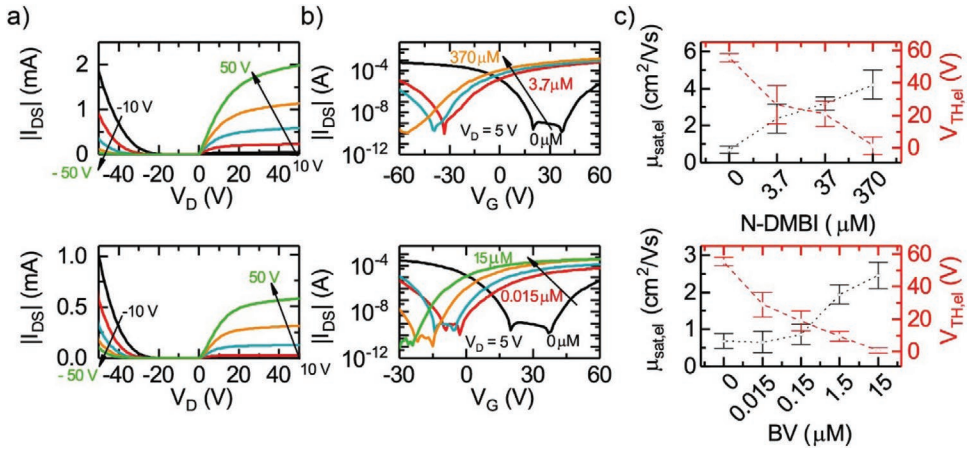

Figure 3. a) Output curves of FETs prepared with HiPCO:P3DDT ink mixed with either 370 µM N-DMBI (top) or with 15 µM BV (bottom). b) Transfer curves of FETs prepared with HiPCO:P3DDT with different concentrations of either N-DMBI (top) or BV (bottom). c) Mobility and V_{TH} of FETs prepared with HiPCO:P3DDT ink with indicated concentrations of N-DMBI (top) or BV (bottom). For each doping concentration, eight devices were measured. The error bars show the standard deviation of the average.

The V_{TH} of the FETs containing BV decreases proportionally to the increase of the BV concentration, reaching the ideal V_{TH} = 0 at a concentration of 15 µM as shown in Figure 3c (bottom). However, the mobility stays constant at low BV concentrations, and only when the concentration of BV increases above 0.15 µM, the electron mobility starts to increase reaching values of 2.5 cm^2 V^{-1} s^1 with the highest concentration investigated. In contrast, FETs fabricated with the addition of N-DMBI show a clear dependence of the mobility on the concentration of the added molecules (Figure 3c, top).[39] Moreover, the overall mobility values of the FETs using N-DMBI are higher than the mobility values obtained by adding BV. An electron mobility up to 4.2 cm^2 V^{-1} s^1 with 0 V threshold is obtained with the maximum N-DMBI concentration (see Figure 3c).

F_4-TCNQ has been used successfully to achieve p-doping in conjugated polymers.[40] Since our HiPCO:P3DDT reference FET (Figure 1b) is hole-dominated as well, we prepared another reference FET to put ourselves in the worst possible conditions. To this end we used a polyfluorene derivative, the atactic poly(9-dodecyl-9-methyl-fluorene-2,7-diyl) (aPF1-12) to select HiPCO tubes. This reference ink in the coplanar structure gives rise to FETs with ambipolar characteristics, as shown in Figure S4, Supporting Information. These ambipolar devices showed hole mobility of 2.7 ± 0.6 cm^2 V^{-1} s^{-1} and electron mobility of 1.3 ± 0.4 cm^2 V^1 s^{-1}.

Figure 4a shows the output curves of the FETs that have been prepared with the HiPCO:P3DDT ink with the addition of 7.97 mM F_4-TCNQ (top) and the HiPCO:aPF1-12 ink to which 1.81 mM F_4-TCNQ was added (bottom). As expected, the

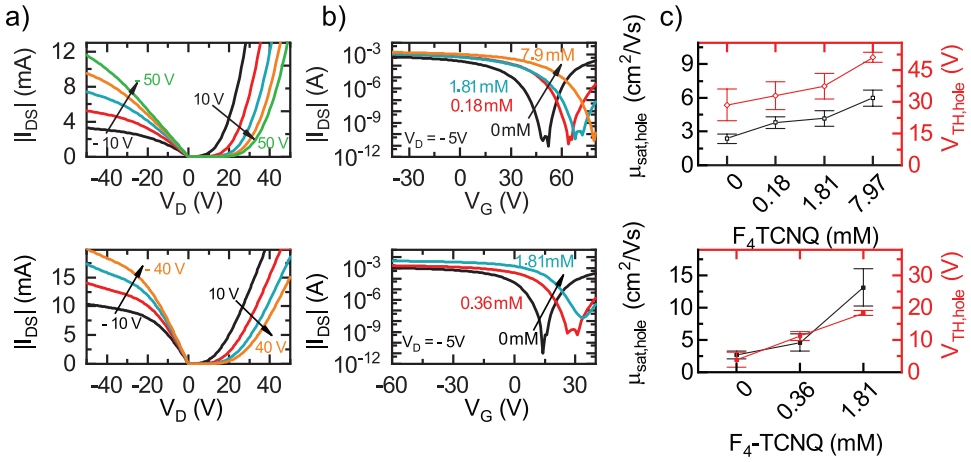

Figure 4. a) Output curves of FETs prepared with the HiPCO:P3DDT ink mixed with 7.97 mM F_4-TCNQ (top), and FETs prepared with HiPCO:aPF1-12 ink mixed with 1.81 mM F_4-TCNQ (bottom). b) Transfer curves of FETs prepared with HiPCO:P3DDT ink mixed with the indicated concentrations of F_4-TCNQ (top) and FETs prepared with HiPCO:aPF1-12 ink mixed with the indicated concentrations of F_4-TCNQ (bottom). c) Mobility and V_{TH} of FETs prepared with HiPCO:P3DDT ink mixed with the indicated concentrations of F_4-TCNQ (top) and of FETs prepared with HiPCO:aPF1-12 ink mixed with indicated concentrations of F_4-TCNQ (bottom). For each doping concentration, eight devices were measured. The error bars show the standard deviation of the average.

addition of F_4-TCNQ resulted in hole dominated FETs, in both the HiPCO:aPF1-12 (Figure 4a, bottom), and the HiPCO:P3DDT sample (Figure 4a, top). Upon increasing the F_4-TCNQ concentration, the transfer curves show a shift of the threshold voltage toward more positive values together with an increased hole current (Figure 4b). Both experimental facts are compatible with a variation of the hole density in the active channel of the FETs with an increased amount of F_4-TCNQ. This is further confirmed by the increased hole mobility in these devices. FETs prepared with the HiPCO:P3DDT ink mixed with 7.97 mM F_4-TCNQ show hole mobility up to 6.0 ± 0.7 $cm^2\ V^{-1}\ s^{-1}$ while FETs prepared with the HiPCO:aPF1-12 ink mixed with 1.81 mM show hole mobility of 13.2 ± 2.9 $cm^2\ V^{-1}\ s^{-1}$.

It is interesting to note that the FETs prepared with the HiPCO:aPF1-12 ink mixed with F_4-TCNQ show a larger increase of the mobility (three times at the same additive concentration) than the one obtained with the HiPCO:P3DDT-doped inks. Considering that the HiPCO: aPF1-12 and HiPCO:P3DDT reference FETs had similar mobility, and that the same HiPCO nanotubes are used to prepare the inks. The difference in mobility of the FETs containing F_4-TCNQ is an indication of a different doping efficiency of the F_4-TCNQ for the two polymers used for the dispersion of the nanotubes. Therefore, we can conclude that the polymer is playing an essential role in the doping of our SWNT inks with F_4-TCNQ.

So far, our results show that the additives change the polarity of the FETs mainly by shifting the V_{TH}. While for the addition of F_4-TCNQ and N-DMBI, there is a simultaneous increase of the mobility and variation of the threshold shift, samples fabricated with BV deviate from this trend and the mobility, in this case, increases only for the highest concentrations.

At this point, it is very important to understand the mechanism involved in the polarity variation and the large mobility increase induced by the addition of the additive in the inks. We identify three possible causes that could induce the V_{TH} variation: i) a trap-limited charge transport,[41] ii) the variation of the density of majority carriers by chemical doping, or iii) the variation of the energy level alignment between either side of the dielectric and the metal electrodes, namely, variations in the flat band potential (V_{FB}).[42]

Our strategy to uncover the mechanism of the V_{TH} shift is to use a staggered (bottom contact, top gate) transistor configuration using a hydroxyl-free dielectric. By avoiding in this way, the interface traps, which negatively affect the performance of SWNT FETs,[34] the large hysteresis present in the coplanar devices (Figure S1, Supporting Information) should disappear allowing to discard the trap limited charge transport as a cause of the V_{TH} shifts.[42] In order to prepare the FETs in the staggered configuration, we used PMMA/Al_xO_x as a dielectric material and evaporated Au as top gate contact as shown in the schematic structure in **Figure 5**a. As expected, these devices (Figure 5b,c) show a large reduction of the hysteresis compared to devices in coplanar configuration (Figure S1, Supporting Information), showing the successful reduction of the trap density at the semiconductor–dielectric interface.

The transfer curves of the HiPCO:P3DDT reference device, and the one of the HiPCO:P3DDT inks containing 15 µM BV or 370 µM N-DMBI are shown in Figure 5b. Also, in this configuration, the transfer curves of the nanotubes doped with BV and

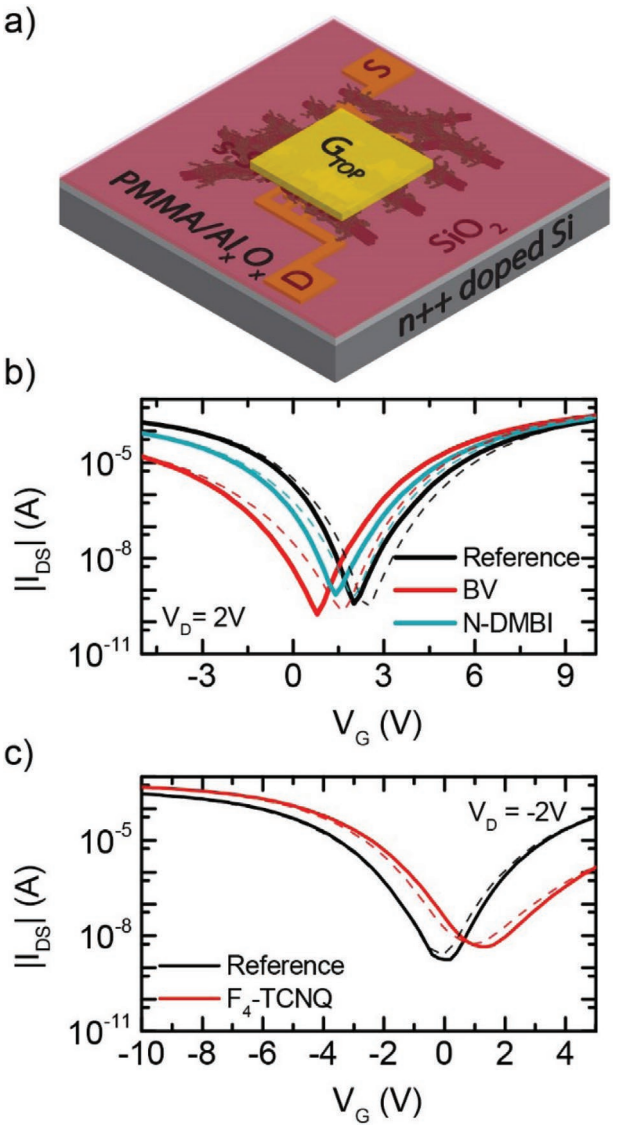

Figure 5. a) Staggered FET structure. b) Comparison of the transfer curves of the reference device fabricated with the HiPCO:P3DDT, and devices prepared with the inks that contain BV and N-DMBI. c) Comparison of the transfer curves of the reference device using HiPCO:P3DDT, and devices prepared with the ink containing F_4-TCNQ. The dashed lines are the backward scans, the difference between forward and backward scan, demonstrate the negligible hysteresis in this device configuration.

N-DMBI are shifting toward more negative values compared with the reference device, while devices containing 7.97 mM of F_4-TCNQ are shifted toward more positive values with respect to the reference (Figure 5c). Even if the qualitative behavior appears similar, the voltage shift is much lower than reported earlier, a reason for this is also the different capacitance of the gate dielectric used in the staggered configuration.

The suppression of the trap-limited transport allows us to differentiate between the other two possible V_{TH} shift mechanisms, namely between changes in the chemical doping or in V_{FB}. Changes in V_{FB} are correlated with the Schottky barrier height (φ_{SB}). A decrease in φ_{SB} improves the extraction of majority carriers, which translates to a reduction of the contact

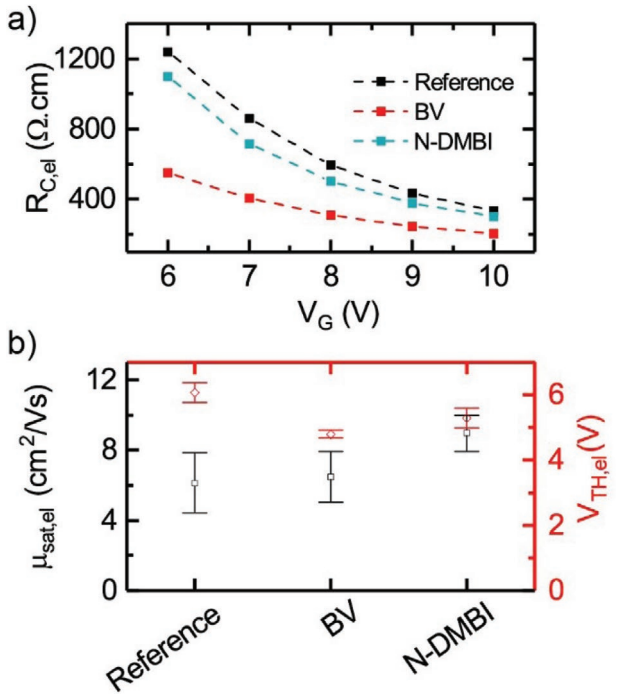

Figure 6. a) Values of the contact resistance (R_c) for the reference device, the N-DMBI and the BV treated SWNTs device. b) Mobility and V_{TH} for the three sample types. For each dopant, eight devices were measured, the error bars show the standard deviation of the average.

resistance (R_c).[36] In the staggered configuration, the R_c extrapolation can be performed more reliably, as the gate is not in contact with the drain/source electrodes.[43]

The relation between the V_{TH} and the φ_{SB} can be seen in the equations defining V_{TH}:

$$V_{TH} = \left(\phi_{ms} - \frac{Q_f}{C_{ox}}\right) + 2\psi_B + \frac{\sqrt{4\varepsilon_s q N_a \psi_B}}{C_{ox}} \quad (1)$$

where V_{TH} is given by the sum of three terms, the first one determines the flat band potential V_{FB} as Φ_{ms} (work function difference between the electrode gate material and the semiconductor) minus Q_f (fixed oxide charge density)/C_{ox} (oxide or dielectric capacitance per area); the second term is twice the bulk potential ($2\Psi_B$). The square-root term is the total depletion-layer charge, where ε_s is the permittivity of the semiconductor and N_a is the acceptor impurity concentration.[44] V_{FB} is related to Φ_{ms}, and in our case, Φ_{ms} determines the value of φ_{SB}.

In order to identify whether the V_{TH} shift in our FETs results from changes in the density of charges or a variation of the V_{FB}, we analyzed the mobility and the R_c of the devices in the staggered configuration.

Figure 6a shows the R_c as a function of gate voltage measured using the transfer line method[38] for the reference device, and for the FETs containing 15 μM BV or 370 μM N-DMBI. The R_c of the FET containing 370 μM N-DMBI shows a slight decrease to 1098 ohm·cm (at V_G = 6 V) from the value of 1237 ohm·cm (at V_G = 6 V) for the reference device. The R_c of the FETs containing 15 μM BV (549 ohm·cm at V_G = 6 V) is reduced over the whole gate voltage range to less than half of the R_c of the reference device.

In Figure 6b, the electron mobility of the three different active layers under investigation are reported along with their threshold voltage. Only the sample treated with N-DMBI shows a significant increase of mobility up to a value of 9.0 ± 1.0 cm^2 V^{-1} s^{-1}, while the sample containing BV shows a mobility of 6.5 ± 1.4 cm^2 V^{-1} s^{-1}, which is very close to the one measured for the reference sample (6.1 ± 1.7 cm^2 V^{-1} s^{-1}).

Interestingly, in the coplanar structure, the introduction of BV resulted in higher mobility of 2.5 ± 0.4 cm^2 V^{-1} s^{-1} versus 0.7 ± 0.2 cm^2 V^{-1} s^{-1} for the reference device. The difference between the planar and staggered device structure suggests that the increase in mobility in the planar structure after BV addition is a consequence of the passivation of surface traps at the dielectric-semiconductor interface.

Therefore, the results reported in Figure 6 are an indication that different mechanisms are involved in the V_{th} shift for BV and N-DMBI. For BV, the reduction of the R_c from 1237 ohm·cm to 549 ohm·cm (at V_G = 6 V) next to the shift in V_{th}, without an increase in mobility indicates a possible variation of the φ_m as the main mechanism for the polarity variation of the FETs. Kelvin probe results showed in Table S1, Supporting Information, point out in the same direction, showing a decrease in the $\varphi_{m,}$ when BV is present on the surface. Opposed to this, the small decrease in the R_c along with the V_{TH} shift and the increase in mobility, in the case of samples containing N-DMBI, could be an indication that the mechanism for the polarity modification is the charge density variation in the active channel. Therefore, we propose that for this additive the change in polarity is caused by molecular doping of the active channel, as was also reported by other authors which have deposited N-DMBI as an extra layer on top of the s-SWNT active layer.[18,45]

We, therefore, proceed to determine the contact resistance, R_c, and the mobility in staggered FETs fabricated with F_4-TCNQ treated HiPCO:P3DDT. Interestingly, the presence of F_4-TCNQ decreases the R_c for holes from 400 ohm·cm to 46 ohm·cm (at V_G = 6 V), a much stronger reduction than in the case of N-DMBI and BV. It is also important to notice that at the same time the hole mobility for HiPCO:P3DDT FETs increases from 5.2 ± 0.5 cm^2 V^{-1} s^{-1} to 6.4 ± 0.5 cm^2 V^{-1} s^{-1} (**Figure 7**a,b). Moreover, a decrease in the V_{TH} is observed as expected when the p-character of the FET is enhanced (Figure 7b).

The substantial reduction of R_c, along with the increase in the mobility and the shift in $V_{TH,}$ suggests that both chemical doping and V_{FB} modification occur in the F_4-TCNQ-containing FETs. However, it is very difficult to disentangle the two effects as the molecular doping can also partially decrease the contact resistance. Moreover, we have seen from the optical investigation of this sample that F_4-TCNQ interacts strongly with both the nanotubes and the polymer, and even the density of the s-SWNT network seems to be affected as shown by the atomic force microscopy micrographs in Figure S5, Supporting Information.

Important to notice that the doping mechanism seems to be mediated by the polymer that is wrapped around the SWNTs, since the increase in mobility depends on the type of conjugated polymer that is used for the selection.[34] The mobility

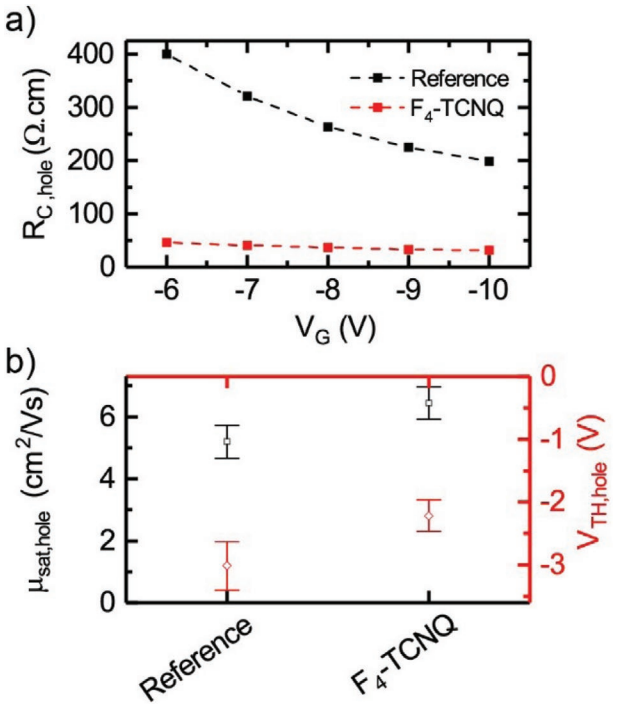

Figure 7. a) Contact resistance values for reference FETs and the devices containing F_4-TCNQ. b) Mobility and V_{TH} for the reference HiPCO:P3DDT sample and the F_4-TCNQ containing FET. For each dopant, eight devices were measured; the error bars show the standard deviation of the average.

is found to increase by a factor five in the case of aPF1-12 wrapped SWNTs and only by a factor of two when P3DDT wrapped SWNTs are employed (Figure 4).

3. Conclusion

We have successfully demonstrated the feasibility of changing the polarity of s-SWNT FETs by mixing BV, N-DMBI, and F_4-TCNQ with the ink obtained by polymer wrapping of SWNTs. The FETs containing BV and N-DMBI exhibit n-type dominated transport and the one with F_4-TCNQ show enhanced p-character. This strategy allows controlling the SWNT FET polarity without extra fabrication steps, but rather by directly modifying the nature of the ink.

The results obtained with FETs in staggered configuration allowed to clarify the mechanism behind the change in polarity, by eliminating the surface trap contribution as a possible cause. In the case of BV, the transistors display lower contact resistance without a concurrent increase in mobility, showing that the most probable mechanism is a modification of the Schottky barrier between the metal contact and the SWNT network. For FETs containing N-DMBI, the substantial increase in mobility and the threshold shift suggests the effective molecular doping of SWNT wrapped polymers.

In the case of F_4-TCNQ, an interplay between molecular doping and work function modification seems to occur. Interestingly different performances are obtained when the dopant is added to HiPCO: aPF1-12 or HiPCO:P3DDT, demonstrating that the polymer wrapping the SWNTs mediates the doping by F_4-TCNQ. Absorption and photoluminescence spectroscopy show the strong interaction of F_4-TCNQ with the carbon nanotube based hybrids.

4. Experimental Section

Polymer Synthesis: The homopolymer P3DDT and aPF1-12 were synthesized as described previously[46,47] and the molecular weights were measured using gel permeation chromatography (GPC) versus narrowly distributed polystyrene standards. P3DDT was obtained after Soxhlet extraction with methanol, acetone, ethyl acetate, and hexane. For the experiments reported herein, the hexane fraction with $M_n = 19.200$ g mol^{-1} and $M_w = 22.300$ g mol^{-1} was used. aPF1-12 was fractionated by Soxhlet extraction with methanol, acetone, ethyl acetate, and chloroform. From the chloroform fraction, a high molecular weight aPF1-12 with M_n = 65.200 g mol^{-1} and $M_w = 116.000$ g mol^{-1} was obtained.

Preparation and Characterization of Semiconducting SWNT Dispersion: HiPCO SWNTs (diameters between 0.8 and 1.2 nm) were purchased from Unidym, Inc. The polymers were solubilized in toluene using a high power ultrasonicator (Misonix 3000) with cup horn bath (output power 69 W) for 10 min, followed by overnight stirring at 60 °C. Subsequently, SWNTs were added to form the SWNT:polymer dispersions with a weight ratio of 1:2 (3 mg of SWNTs, 6 mg of polymer, 15 mL of toluene). These solutions were then sonicated for 2 h at 69 W and 16 °C.

After ultrasonication, the dispersions were centrifuged at 30 000 rpm (109 000 *g*) for 1 h in an ultracentrifuge (Beckman Coulter Optima XE-90; rotor: SW55Ti) to remove all the remaining bundles and heavy-weight impurities. After the centrifugation, the highest density components precipitate at the bottom of the centrifugation tube, while the low-density components, including small bundles and individualized SWNTs wrapped by the polymer, and free polymer chains, remain in the upper part (the supernatant).

One extra step of ultracentrifugation was implemented to decrease the amount of free polymer in solution (enrichment). For this purpose, the supernatant obtained after the first ultracentrifugation is centrifuged for 5 h at 55 000 rpm (367 000 *g*), where the individualized s-SWNTs precipitates to form a pellet, and the free polymer remains in the supernatant. Finally, the pellet is re-dispersed by sonication in the solvent of choice in this case o-xylene.[48]

Preparation of Doped Polymer-Wrapped SWNTs: All dopant concentrations were determined based on the maximum amount of material that were able to disperse on O-xylene without affecting the homogeneity of the HiPCO:polymer solutions. Benzyl viologen dichloride powder (51 mg) as received from Sigma Aldrich was dissolved in water (4.5 mL) and o-xylene (9 mL). Subsequently, sodium borohydride (97 mg) was added to the solution as a catalytic reducing agent. The reaction was left overnight, after which the solution changed color from purple to bright yellow. Then, the BV product in o-xylene was mixed with the SWNT ink at the corresponding volume percentages.

4-(2,3-Dihydro-1,3-dimethyl-1H-benzimidazol-2-yl)-*N*,*N*-dimethylbenzenamine (N-DMBI) from Sigma Aldrich was dissolved in the o-xylene by stirring at 80 °C. The solutions, both in o-xylene were mixed, the SWNT ink at the concentrations mentioned in the main text. The solutions were heated at 90 °C for 3 min to form an aggregated state of N-DMBI.[49] Subsequently, the solutions were sonicated for 15 min at 78 W and the temperature was decreased gradually from 25 to 18 °C during the sonication.

2,3,5,6-Tetrafluoro-7,7,8,8-tetracyanoquinodimethane (F_4-TCNQ) from sigma Aldrich was dissolved in the SWNTs ink at the required concentrations. To assure the dopant interaction with the SWNTs, the solutions were sonicated for 15 min at 78 W and the temperature was decreased gradually from 25 to 18 °C during the sonication.

Field Effect Transistors Fabrication and Electrical Measurements: Field effect transistors were fabricated on silicon substrates with a thermally grown SiO_2 dielectric layer (230 nm thickness). Source and drain bottom electrodes (10 nm ITO/30 nm Au) were lithographically

patterned forming an interdigitated channel of 20–2.5 µm length and 2 mm width. The different SWNTs dispersions tested were deposited by blade coating (Zehntner ZAA 2300 Automatic film applicator coater) using 8 µL of s-SWNT with a concentration of 0.2 mg mL^{-1} and a blade speed of 3 mm s^{-1} at 70 °C. The procedure was repeated twice to achieve sufficient SWNT coverage. After deposition, the samples were annealed at 160 °C for 2 h in N_2 environment to evaporate the remaining solvent. The final mobility of the samples is strongly dependent on the concentration, therefore the SWNTs concentration was kept constant for all the experiments.

Staggered Top Gate Bottom Contact Configuration: PMMA with M_w = 120.000 g mol^{-1} was purchased from Sigma Aldrich. 10 nm layer of PMMA (5 mg mL^{-1} in Acetonitrile) was deposited by spin coating at 3000 rpm on top of the active layer of the FET. The first step was followed by removing the residual solvent at 115 °C for 30 min. Then, Al_xO_x was deposited by Atomic layer deposition using a Picosun R-200 Advanced ALD System. As precursor and reagent Trimethylaluminium (TMA) and DI H_2O were used. The deposition was performed at 100 °C. TMA pulse- and purge times were 0.1 and 8 s at 150 sccm. H_2O pulse- and purge times were 0.1 and 8 s at 200 sccm. In total 600 cycles were performed, resulting in a thickness of 47 nm. The device structure was finalized by the thermal evaporation of 100 nm Au layer as the top contact.

Electrical measurements were performed using a probe station placed in a nitrogen-filled glovebox at room temperature under dark conditions. The probe station was connected to an Agilent E5262A Semiconductor Parameter Analyzer. All devices were fabricated and measured in a nitrogen-filled glovebox, without being exposed to air. The reported charge carrier mobilities were extracted from the I_{DS}-V_G transfer characteristics in the saturation regime where the average was calculated from eight devices. The value of the saturation mobility is an overestimation compared to the value of the linear mobility as it is showed in Figure S6, Supporting Information. The gate capacitance was the parallel plate capacitance value corrected for the linear density of CNT network (Figure S5, Supporting Information), and quantum capacitance of SWCNTs as described by Cao et al.[50]

The contact resistance values were obtained from the IV characteristic using the transfer length method, as described by Natali et al.[36] The measured channel length devices were 20, 10, 5, and 2.5 µm with the gate voltage from 6 to 10 V for electrons and −6 to −10 V for holes. Further details can be found in Figures S7 and S8, Supporting Information.

Optical Characterization of the Semiconducting SWNT Dispersion: Optical measurements were performed to check the concentration of the carbon nanotubes selected by the polymers and to observe the effect of doping molecules. Absorption spectra were recorded by a UV–Vis–NIR spectrophotometer (Shimadzu UV-3600). For the PL measurement, the samples were excited at approximately 400 nm by the second harmonic and at 800 nm by fundamental mode of a mode-locked Ti:Sapphire laser (Mira 900, Coherent). The laser power was controlled by a variable neutral density filter. The PL decays were recorded by a Hamamatsu streak camera working in a synchroscan mode (time resolution approximately 2 ps). Lifetimes were fitted using exponential functions such as $I = \sum_i A_i \exp(-t/\tau_i)$. When only one lifetime is reported, the best fit could be achieved with a monoexponential function; otherwise, a biexponential function was used. The PL spectra were corrected for the spectral response of the setup using a calibrated light source.

Supporting Information

Supporting Information is available from the Wiley Online Library or from the author.

Acknowledgements

The authors are thankful to A. Kamp and T. Zaharia for technical support. This work is part of the research program of the Netherlands Organisation for Scientific Research (NWO). This is a publication of the FOM-focus group "Next Generation Organic Photovoltaics" participating in the Dutch Institute for Fundamental Energy Research (DIFFER).

Conflict of Interest

The authors declare no conflict of interest.

Keywords

doping, field-effect transistors, polarity control, polymer wrapping, single-walled carbon nanotubes

Received: July 29, 2019
Revised: September 13, 2019
Published online: November 29, 2019

[1] A. D. Franklin, *Nature* **2013**, *498*, 443.
[2] A. Javey, J. Guo, Q. Wang, M. Lundstrom, H. Dai, *Nature* **2003**, *424*, 654.
[3] R. Martel, T. Schmidt, H. R. Shea, T. Hertel, P. Avouris, *Appl. Phys. Lett.* **1998**, *73*, 2447.
[4] S. J. Tans, A. R. M. Verschueren, C. Dekker, *Nature* **1998**, *393*, 49.
[5] Y. Cao, S. Cong, X. Cao, F. Wu, Q. Liu, M. R. Amer, C. Zhou, *Top. Curr. Chem.* **2017**, *375*, 75.
[6] R. H. Baughman, A. A. Zakhidov, W. A. de Heer, *Science* **2002**, *297*, 787.
[7] E. S. Snow, J. P. Novak, P. M. Campbell, D. Park, *Appl. Phys. Lett.* **2003**, *82*, 2145.
[8] L. Hu, D. S. Hecht, G. Grüner, *Chem. Rev.* **2010**, *110*, 5790.
[9] A. Nish, J.-Y. Hwang, J. Doig, R. J. Nicholas, *Nat. Nanotechnol.* **2007**, *2*, 640.
[10] S. K. Samanta, M. Fritsch, U. Scherf, W. Gomulya, S. Z. Bisri, M. A. Loi, *Acc. Chem. Res.* **2014**, *47*, 2446.
[11] V. Derenskyi, W. Gomulya, J. M. S. Rios, M. Fritsch, N. Fröhlich, S. Jung, S. Allard, S. Z. Bisri, P. Gordiichuk, A. Herrmann, U. Scherf, M. A. Loi, *Adv. Mater.* **2014**, *26*, 5969.
[12] W. Gomulya, V. Derenskyi, E. Kozma, M. Pasini, M. A. Loi, *Adv. Funct. Mater.* **2015**, *25*, 5858.
[13] S. P. Schießl, N. Fröhlich, M. Held, F. Gannott, M. Schweiger, M. Forster, U. Scherf, J. Zaumseil, *ACS Appl. Mater. Interfaces* **2015**, *7*, 682.
[14] S. Z. Bisri, J. Gao, V. Derenskyi, W. Gomulya, I. Iezhokin, P. Gordiichuk, A. Herrmann, M. A. Loi, *Adv. Mater.* **2012**, *24*, 6147.
[15] W. J. Yu, U. J. Kim, B. R. Kang, I. H. Lee, E.-H. Lee, Y. H. Lee, *Nano Lett.* **2009**, *9*, 1401.
[16] D. Bode, C. Rolin, S. Schols, M. Debucquoy, S. Steudel, G. H. Gelinck, J. Genoe, P. Heremans, *IEEE Trans. Electron Devices* **2010**, *57*, 201.
[17] S. D. Vusser, J. Genoe, P. Heremans, *IEEE Trans. Electron Devices* **2006**, *53*, 601.
[18] H. Wang, P. Wei, Y. Li, J. Han, H. R. Lee, B. D. Naab, N. Liu, C. Wang, E. Adijanto, B. C.-K. Tee, S. Morishita, Q. Li, Y. Gao, Y. Cui, Z. Bao, *Proc. Natl. Acad. Sci. USA* **2014**, *111*, 4776.
[19] Y. Ren, J.-Q. Yang, L. Zhou, J.-Y. Mao, S.-R. Zhang, Y. Zhou, S.-T. Han, *Adv. Funct. Mater.* **2018**, *28*, 1805599.
[20] Y. Ren, X. Yang, L. Zhou, J.-Y. Mao, S.-T. Han, Y. Zhou, *Adv. Funct. Mater.* **2019**, *29*, 1902105.
[21] T. Lei, L.-L. Shao, Y.-Q. Zheng, G. Pitner, G. Fang, C. Zhu, S. Li, R. Beausoleil, H.-S. P. Wong, T.-C. Huang, K.-T. Cheng, Z. Bao, *Nat. Commun.* **2019**, *10*, 1.
[22] L. Xiang, H. Zhang, G. Dong, D. Zhong, J. Han, X. Liang, Z. Zhang, L.-M. Peng, Y. Hu, *Nat. Electron.* **2018**, *1*, 237.

[23] M. L. Geier, P. L. Prabhumirashi, J. J. McMorrow, W. Xu, J.-W. T. Seo, K. Everaerts, C. H. Kim, T. J. Marks, M. C. Hersam, *Nano Lett.* **2013**, *13*, 4810.
[24] J. L. Blackburn, S. D. Kang, M. J. Roos, B. Norton-Baker, E. M. Miller, A. J. Ferguson, *Adv. Electron. Mater.* **2019**, *5*, 1800910.
[25] B. A. MacLeod, N. J. Stanton, I. E. Gould, D. Wesenberg, R. Ihly, Z. R. Owczarczyk, K. E. Hurst, C. S. Fewox, C. N. Folmar, K. H. Hughes, B. L. Zink, J. L. Blackburn, A. J. Ferguson, *Energy Environ. Sci.* **2017**, *10*, 2168.
[26] J. Zhang, C. Wang, Y. Fu, Y. Che, C. Zhou, *ACS Nano* **2011**, *5*, 3284.
[27] C. Wang, K. Ryu, A. Badmaev, J. Zhang, C. Zhou, *ACS Nano* **2011**, *5*, 1147.
[28] M. H. Yang, K. B. K. Teo, L. Gangloff, W. I. Milne, D. G. Hasko, Y. Robert, P. Legagneux, *Appl. Phys. Lett.* **2006**, *88*, 113507.
[29] M. L. Geier, K. Moudgil, S. Barlow, S. R. Marder, M. C. Hersam, *Nano Lett.* **2016**, *16*, 4329.
[30] J. M. Salazar-Rios, W. Gomulya, V. Derenskyi, J. Yang, S. Z. Bisri, Z. Chen, A. Facchetti, M. A. Loi, *Adv. Electron. Mater.* **2015**, *1*, 8.
[31] A. G. Shulga, V. Derenskyi, J. M. Salazar-Rios, D. N. Dirin, M. Fritsch, M. V. Kovalenko, U. Scherf, M. A. Loi, *Adv. Mater.* **2017**, *29*, 35.
[32] H. W. Lee, Y. Yoon, S. Park, J. H. Oh, S. Hong, L. S. Liyanage, H. Wang, S. Morishita, N. Patil, Y. J. Park, J. J. Park, A. Spakowitz, G. Galli, F. Gygi, P. H.-S. Wong, J. B.-H. Tok, J. M. Kim, Z. Bao, *Nat. Commun.* **2011**, *2*, 541.
[33] W. Gomulya, J. M. S. Rios, V. Derenskyi, S. Z. Bisri, S. Jung, M. Fritsch, S. Allard, U. Scherf, M. C. Dos Santos, M. A. Loi, *Carbon* **2015**, *84*, 66.
[34] S. P. Schiessl, N. Fröhlich, M. Held, F. Gannott, M. Schweiger, M. Forster, U. Scherf, J. Zaumseil, *ACS Appl. Mater. Interfaces* **2015**, *7*, 682.
[35] S. Kahmann, J. M. Salazar Rios, M. Zink, S. Allard, U. Scherf, M. C. dos Santos, C. J. Brabec, M. A. Loi, *J. Phys. Chem. Lett.* **2017**, *8*, 5666.
[36] S. M. Kim, J. H. Jang, K. K. Kim, H. K. Park, J. J. Bae, W. J. Yu, I. H. Lee, G. Kim, D. D. Loc, U. J. Kim, E.-H. Lee, H.-J. Shin, J.-Y. Choi, Y. H. Lee, *J. Am. Chem. Soc.* **2009**, *131*, 327.
[37] W. Gao, A. Kahn, *J. Appl. Phys.* **2003**, *94*, 359.
[38] K. H. Eckstein, H. Hartleb, M. M. Achsnich, F. Schöppler, T. Hertel, *ACS Nano* **2017**, *11*, 10401.
[39] A. Higgins, S. K. Mohapatra, S. Barlow, S. R. Marder, A. Kahn, *Appl. Phys. Lett.* **2015**, *106*, 163301.
[40] I. E. Jacobs, A. J. Moulé, *Adv. Mater.* **2017**, *29*, 1703063.
[41] G. Horowitz, R. Hajlaoui, H. Bouchriha, R. Bourguiga, M. Hajlaoui, *Adv. Mater.* **1998**, *10*, 923.
[42] G. Horowitz, P. Lang, M. Mottaghi, H. Aubin, *Adv. Funct. Mater.* **2004**, *14*, 1069.
[43] D. Natali, M. Caironi, *Adv. Mater.* **2012**, *24*, 1357.
[44] S. M. Sze, K. K. Ng, *Physics of Semiconductor Devices*, John Wiley & Sons, New York **2006**, pp. 293–373.
[45] B. D. Naab, S. Guo, S. Olthof, E. G. B. Evans, P. Wei, G. L. Millhauser, A. Kahn, S. Barlow, S. R. Marder, Z. Bao, *J. Am. Chem. Soc.* **2013**, *135*, 15018.
[46] R. S. Loewe, S. M. Khersonsky, R. D. McCullough, *Adv. Mater.* **1999**, *11*, 250.
[47] B. M. Grell, W. Knoll, D. Lupo, A. Meisel, T. Miteva, D. Neher, H. Nothofer, U. Scherf, A. Yasuda, *Adv. Mater.* **1999**, *11*, 671.
[48] W. Talsma, A. A. Sengrian, J. M. Salazar-Rios, H. Duim, M. Abdu-Aguye, S. Jung, S. Allard, U. Scherf, M. A. Loi, *Adv. Electron. Mater.* **2019**, *5*, 1900288.
[49] P. Wei, J. H. Oh, G. Dong, Z. Bao, *J. Am. Chem. Soc.* **2010**, *132*, 8852.
[50] Q. Cao, M. Xia, C. Kocabas, M. Shim, J. A. Rogers, S. V. Rotkin, *Appl. Phys. Lett.* **2007**, *90*, 2005.